

# Growth of $\text{TiO}_2$ nanoparticles in thermally evaporated fatty amine thin films by a method of ion entrapment<sup>†</sup>

S. Shiv Shankar, Debabrata Rautaray, Renu Pasricha, Neela R. Pavaskar, Anandrao B. Mandale and Murali Sastry\*

Materials Chemistry Division, National Chemical Laboratory, Pune – 411008, India 30050.  
E-mail: sastry@ems.ncl.res.in; Fax: +91 20 5893952/5893044; Tel: +91 20 5893044

Received 3rd February 2003, Accepted 6th March 2003  
First published as an Advance Article on the web 14th March 2003

The synthesis of titania nanoparticles within thermally evaporated octadecylamine (ODA) thin films is described. Synthesis of the nanoparticles was achieved by electrostatically entrapping  $\text{TiF}_6^{2-}$  ions in thin films of the fatty amine by a simple immersion technique followed by *in-situ* hydrolysis of the metal ions. Without any further heat treatment, it was observed that titania nanoparticles of the brookite polymorph were formed within the film. By this simple procedure, uniformly distributed fairly monodisperse titania nanoparticles of *ca.* 4 nm diameter were synthesized within the lipid matrix and investigated using a host of techniques.

## Introduction

Metal oxides constitute an important class of materials of high technological importance. They have numerous applications in a wide range of areas, from day-to-day commercial utilities to biomedicine. In particular, nanoparticles of titania are very important and have attracted much interest both from fundamental and applied perspectives due to their very unique properties compared to their bulk forms.<sup>1</sup> Nanoparticles of titania are used as photocatalysts,<sup>2–5</sup> in sensors,<sup>6,7</sup> optical devices,<sup>8</sup> electrochromic devices<sup>9</sup> and in lithium batteries.<sup>10</sup> For many of the above applications it is required to synthesize nanoparticulate thin films of titania in a reproducible manner; examples of some experimental methods include self-assembly<sup>11</sup> and the Langmuir–Blodgett (LB) technique.<sup>12,13</sup>

In this laboratory, we have used electrostatic interactions as a means of synthesizing/assembling nanomaterials in thermally evaporated lipid films. This may be accomplished in two ways. In the first method, metal ions may be entrapped in thermally evaporated lipid films<sup>14</sup> and thereafter, reduced/chemically treated to yield metal or metal sulfide nanoparticles within the lipid matrix. This approach has been used with success in the growth of patterned assemblies of nanoparticles of gold,<sup>15</sup> silver<sup>16</sup> and CdS quantum dots<sup>17</sup> on a variety of solid supports. In a derivative of the above method, metal ions may be replaced with charged nanoparticles and nano-lipid composite structures may be obtained by direct electrostatic entrapment of preformed and functionalized nanoparticles in thermally evaporated ionizable lipid films.<sup>18</sup> As part of our ongoing studies on the use of thermally evaporated lipid films in the synthesis of inorganic nanostructures, we have recently attempted to extend the methodology based on metal ion entrapment to realizing nanoparticles of metal oxides. In this paper, we describe the synthesis of titania nanoparticles ( $\sim$ 4 nm diameter) of good monodispersity in thermally evaporated films of a fatty amine. The procedure is extremely simple and involves immersion of thermally evaporated thin films of octadecylamine (ODA) deposited on suitable solid substrates into a solution of  $\text{K}_2\text{TiF}_6$  under acidic conditions.

Electrostatic interaction between  $\text{TiF}_6^{2-}$  ions in solution and protonated amine molecules in the thermally evaporated amine film drives the immobilization of the metal ions in the lipid matrix. Thereafter, hydrolysis of the ODA– $\text{TiF}_6$  composite film leads to the formation of titania nanoparticles within the lipid matrix. A salient feature of the work is that the titania nanoparticles thus obtained are predominantly in the brookite phase. It is well known that preparing brookite nanoparticles in thin film form is relatively difficult<sup>19,20</sup> and has hitherto been achieved in vacuum deposited films<sup>21</sup> and by electrochemical oxidation of titanium electrodes.<sup>22,23</sup> Presented below are details of the investigation.

## Experimental

250 Å thick octadecylamine (ODA,  $\text{CH}_3(\text{CH}_2)_{17}\text{NH}_2$ ) films were deposited on Si(111) wafers, quartz pieces, gold-coated 6 MHz AT cut quartz crystals and carbon-coated TEM copper grids by thermal evaporation in an Edwards E306A coating system equipped with a liquid nitrogen trap. The pressure during the film deposition was better than  $1 \times 10^{-7}$  Torr. The film thickness/deposition rate was monitored *in situ* by quartz crystal microgravimetry (QCM). QCM measurements of the kinetics of entrapment of  $\text{TiF}_6^{2-}$  ions in the ODA films were carried out by immersing the ODA film deposited on quartz crystals in  $10^{-3}$  M  $\text{K}_2\text{TiF}_6$  solution (pH 3.6) for different times and measuring the frequency change *ex-situ* after thorough washing of the crystals in distilled water and drying. The exact time of drying of the ODA-coated quartz crystal after each cycle of immersion was extremely important. During immersion of the film in the electrolyte solution, the lipid bilayers swell leading to a large uptake of water. After removal of the film from solution, the frequency of the ODA-coated quartz crystal was monitored as a function of time to record evaporation of entrapped water from the film. It was observed that drying the film for 10 min resulted in stabilization of the crystal frequency indicating complete evaporation of water in this time interval and consequently, the film was dried for 15 min prior to each successive immersion cycle. It may be mentioned here that the frequency with which the QCM measurements were carried out (by varying the time interval between measurements) did not result in a significant difference in the ion mass uptake kinetics. The change in the quartz crystal resonance frequency was measured using an Edwards FTM5 frequency

†Electronic supplementary information (ESI) available: Fig. S1: XPS F 2p core level spectra recorded from the ODA– $\text{TiF}_6$  composite film before (curve 1) and after hydrolysis (curve 2). See <http://www.rsc.org/suppdata/jm/b3/b301314f/>

counter that had a frequency resolution and stability of  $\pm 1$  Hz. For the 6 MHz crystal used in this study, this yields a mass resolution of  $12 \text{ ng cm}^{-2}$ . The frequency change was converted to a mass loading using the Sauerbrey equation.<sup>24</sup> The mass change in the ODA–TiF<sub>6</sub> composite film was thereafter monitored during immersion of the film in 1% ammonia solution held at 50 °C. The optimum times of immersion of the ODA films in K<sub>2</sub>TiF<sub>6</sub> and ammonia solutions as determined from QCM measurements was used in the preparation of titania nanoparticle films on other substrates for further analysis. Optical absorption spectroscopy studies of the ODA–titania nanoparticle films on quartz were performed on a Hewlett–Packard HP 8542 A diode array spectrophotometer operated at a resolution of 2 nm. X-Ray photoemission spectroscopy (XPS) analysis of the ODA–TiF<sub>6</sub> and ODA–titania nanoparticle films on Si(111) wafers were carried out on a VG MicroTech ESCA 3000 instrument at a pressure better than  $1 \times 10^{-9}$  Torr. The general scan and C 1s and Ti 2p core level spectra were recorded with un-monochromatized Mg-K $\alpha$  radiation (photon energy = 1253.6 eV) at a pass energy of 50 eV and electron take-off angle (angle between electron emission direction and surface plane) of 60°. The overall resolution of measurement is thus  $\sim 1$  eV for the XPS measurements. The core level spectra were background corrected using the Shirley algorithm and the chemically distinct species resolved using a nonlinear least squares procedure. The core level binding energies (BEs) were aligned with the adventitious carbon binding energy of 285 eV. Transmission electron microscopy (TEM) measurements of the ODA–titania nanoparticle films on carbon-coated TEM grids were carried out on a JEOL Model 1200EX instrument operated at an accelerating voltage of 120 kV. X-Ray diffraction (XRD) measurements of the ODA–TiF<sub>6</sub> as well as the ODA–titania nanoparticle composite films were done on a Philips PW 1830 instrument operating at a voltage of 40 kV and a current of 30 mA with Cu-K $\alpha$  radiation.

## Results and discussion

The kinetics of incorporation of TiF<sub>6</sub><sup>2-</sup> ions into a 250 Å thick ODA thin film during immersion in  $10^{-3}$  M K<sub>2</sub>TiF<sub>6</sub> solution was followed by QCM and the data obtained is shown in Fig. 1(A). It is observed that there is a fairly rapid mass increase due to electrostatically driven diffusion of the TiF<sub>6</sub><sup>2-</sup> ions into the ODA matrix, the equilibration of the metal ion concentration in the ODA matrix occurring within *ca.* 3 h of immersion. As mentioned in the introductory section, the uptake of TiF<sub>6</sub><sup>2-</sup> ions in ODA is to a large extent driven by electrostatic interaction between the negatively charged TiF<sub>6</sub><sup>2-</sup> ions and the amine groups of ODA thin film which are positively charged under the pH conditions of the solution (pH 3.6). During the second cycle of immersion of the composite film in 1% ammonia solution at 50 °C to facilitate the hydrolysis of TiF<sub>6</sub><sup>2-</sup> ions entrapped in ODA film, an additional mass increase in the composite film was observed (Fig. 1(A)). Hydrolysis of the ODA–TiF<sub>6</sub> composite film would lead to the formation of TiO<sub>2</sub> which has lower molecular weight than the already existing TiF<sub>6</sub><sup>2-</sup> ions and consequently, the QCM plot should show a decrease in mass uptake during hydrolysis contrary to the observed mass increase. A couple of factors could be responsible for this observation. The formation of TiO<sub>2</sub>, an uncharged product, would lead to freeing the protonated amine groups in the host and their possible complexation with F<sup>-</sup> ions liberated during the hydrolysis of TiF<sub>6</sub><sup>2-</sup> ions. This process of formation of  $-\text{NH}_3^+ \text{F}^-$  complexes and TiO<sub>2</sub> could explain the mass increase observed during hydrolysis. However, XPS analysis of the ODA–TiF<sub>6</sub> films before and after hydrolysis (see section on XPS analysis) clearly showed that there was a significant reduction in the F 2p core level signal

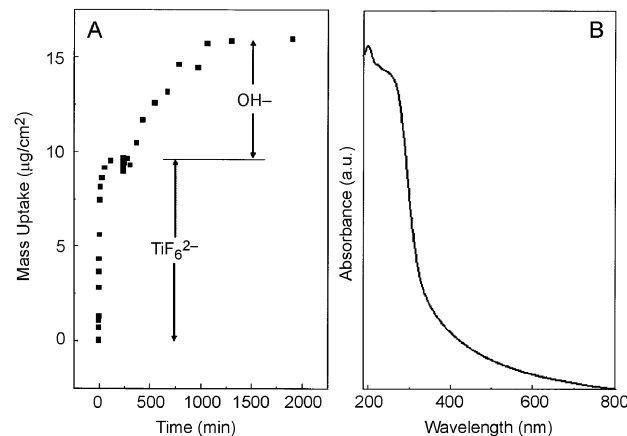
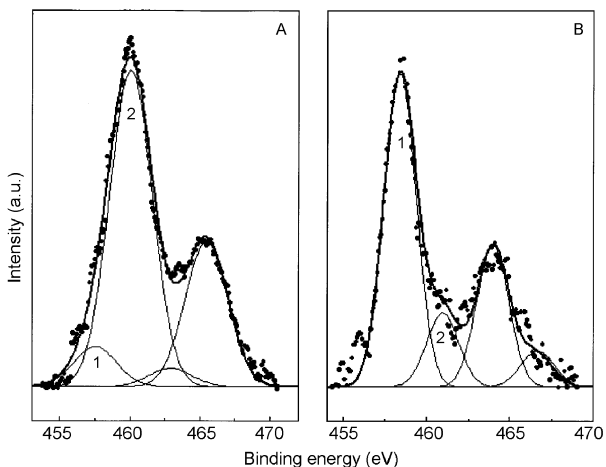


Fig. 1 (A) QCM mass uptake kinetics for a 250 Å thick ODA film during immersion in  $10^{-3}$  M K<sub>2</sub>TiF<sub>6</sub><sup>2-</sup> solution and its subsequent immersion in 1% ammonia solution at 50 °C. (B) Optical absorption spectrum of hydrolyzed TiF<sub>6</sub><sup>2-</sup> entrapped in a 250 Å thick ODA film on quartz.

indicating loss of F<sup>-</sup> ions from the lipid matrix. Another possible explanation for the mass increase after hydrolysis is a large change in the acoustic properties of the ODA–TiF<sub>6</sub> composite film after formation of TiO<sub>2</sub>. The ODA–TiF<sub>6</sub> precursor film would be relatively 'soft' compared to the ODA–TiO<sub>2</sub> film, which has a significant inorganic component to it. We believe the presence of TiO<sub>2</sub> in the ODA matrix would lead to the film becoming 'stiffer' acoustically. In the present measuring mode, the analysis makes no allowance for such a change in the acoustic properties and treats the film after hydrolysis as being similar to the precursor film. This could lead to the anomalous mass increase observed. Efforts are currently underway in this laboratory to estimate changes in the acoustic properties of organo–inorganic composite films based on detailed QCM, ellipsometry and chemical analysis by XPS, and will be dealt with in a future publication. In any case, changes in the apparent 'mass' of the film with time may be viewed indirectly as indicating changes in the ODA–TiF<sub>6</sub> film during hydrolysis and will be viewed in this sense. This cycle of hydrolysis of the entrapped TiF<sub>6</sub><sup>2-</sup> ions occurred in a time period of approximately 12.5 h. The optimum times of immersion of the ODA films in K<sub>2</sub>TiF<sub>6</sub> and ammonia solutions determined from the QCM measurements, *i.e.*, 3 h in K<sub>2</sub>TiF<sub>6</sub> and 12.5 h in 1% ammonia solution, respectively, were used in the preparation of ODA–TiF<sub>6</sub> and ODA–titania nanoparticle samples for additional studies.

The optical absorption spectrum recorded from a 250 Å thick ODA film after entrainment of TiF<sub>6</sub><sup>2-</sup> ions and hydrolysis is shown in Fig. 1(B). It is observed that the film exhibits a sharp absorption edge at *ca.* 350 nm (3.6 eV). The band gap for bulk titania is 3.2 eV<sup>25</sup> and therefore the existence of an absorption edge blue-shifted relative to the bulk counterpart is indicative of the formation of nanoscale titania in the ODA matrix. The blue-shift observed occurs due to quantum confinement effects and is a standard signature of the formation of nanoparticles.<sup>25</sup>

A detailed chemical characterization of the ODA film on Si(111) wafers was effected at different stages of treatment. Fig. 2 shows the XPS Ti 2p core level spectra recorded from a 250 Å thick ODA film after entrainment of TiF<sub>6</sub><sup>2-</sup> ions (A) and after hydrolysis (B). In both cases, the Ti 2p signal had to be resolved into two chemically shifted spin–orbit pairs. In the case of the ODA–TiF<sub>6</sub> composite film, the binding energies of the chemically distinct Ti 2p<sub>3/2</sub> components were found from the fitting analysis to be 457.6 (1) and 460.1 eV (2). The intensity of the low BE component is much smaller than the 460.1 eV component in the as-prepared ODA–TiF<sub>6</sub> film.



**Fig. 2** XPS Ti 2p core level spectra deconvoluted into two chemically distinct species and their corresponding spin-orbit components: (A) after entrainment of  $\text{TiF}_6^{2-}$  ions into a 250 Å thick ODA film and (B) after hydrolysis of  $\text{TiF}_6^{2-}$  entrapped in the 250 Å thick ODA film.

The 457.6 eV BE agrees well with the values obtained by us in an earlier study of  $\text{TiO}_2$  nanoparticles formed in solution.<sup>25</sup> The high BE component is clearly due to coordination of titanium atoms to a more electronegative element and is assigned to electron emission from the  $\text{TiF}_6^{2-}$  ions in the ODA matrix. The XPS results of Fig. 2(A) thus clearly show that while the titanium ions in the ODA matrix are present predominantly as  $\text{TiF}_6^{2-}$  ions, a very small percentage of the titanium ions undergo hydrolysis to yield a  $\text{TiO}_2$  phase in the as-prepared sample. Fig. 2(B) shows a similar analysis of the Ti 2p core level carried out on the ODA– $\text{TiF}_6$  composite film after hydrolysis. It is clearly seen that the low BE component (BE = 458 eV) has increased significantly in intensity relative to the high BE (BE = 461 eV) component. This indicates that a large fraction of the  $\text{TiF}_6^{2-}$  ions have undergone hydrolysis and have transformed to titania. As shown from the UV-vis measurements of Fig. 1(B), the outcome of the hydrolysis reaction is clearly formation of quantum size titania nanoparticles. It would be interesting to follow the fate of the  $\text{F}^-$  ions after hydrolysis. There is a possibility that the  $\text{F}^-$  ions could complex with the  $-\text{NH}_3^+$  groups in the ODA matrix after hydrolysis leading to a mass increase in the film as suggested by the QCM results (Fig. 1(A)). Fig. S1 in the ESI† shows the XPS F 2p core level spectra recorded from the ODA– $\text{TiF}_6$  composite film before (curve 1) and after hydrolysis (curve 2). A significant reduction in the F 2p signal intensity is observed on hydrolysis indicating that the  $\text{F}^-$  ions do not remain within the ODA matrix.

While in principle it is possible to make a rough estimate of the titania nanoparticle size from the shift in the absorption edge relative to bulk titania, a more direct analysis based on TEM would be desirable. Fig. 3(A) shows a representative TEM micrograph recorded from a 250 Å thick ODA film deposited on carbon-coated TEM grids after one cycle of  $\text{TiF}_6^{2-}$  entrainment and hydrolysis. It can be seen from this figure that there is a very high concentration of nanoparticles uniformly distributed over the surface of the film. The particles are fairly uniform in size, an analysis of which yields an average diameter of  $\sim 4$  nm. Selected area electron diffraction (SAED) analysis of the nanoparticles shown in Fig. 3(A) yielded a sharp diffraction pattern (Fig. 3(B)) indicating that the particles are crystalline. The diffraction rings could be indexed based on the brookite structure of titania, further evidence of which is provided by XRD studies of the films presented below.

The inset of Fig. 4 shows the XRD pattern recorded from a 250 Å thick ODA film on an Si(111) substrate after entrainment of  $\text{TiF}_6^{2-}$  ions. The diffraction pattern shows sharp Bragg (00l) reflections with a characteristic odd–even intensity oscillation that is symptomatic of lamellar c-axis ordering of the titanium ions in the ODA matrix.<sup>14</sup> From the separation between the (00l) Bragg reflections, the bilayer thickness in the ODA– $\text{TiF}_6$  composite was calculated to be *ca.* 50.9 nm. This repeat distance is in good agreement with the dimensions of the ODA molecule and the  $\text{TiF}_6^{2-}$  complex. The XRD pattern recorded from the ODA– $\text{TiF}_6$  composite film after hydrolysis is shown in the main part of Fig. 4. It can be seen from this figure that there are a number of Bragg reflections (which were absent prior to the hydrolysis step) indicating that the titania nanoparticles are quite crystalline. Analysis of the diffraction pattern indicated that the Bragg reflections correspond mostly to the brookite phase and to a small extent to the rutile phase. The various Bragg reflections have been indexed in Fig. 4 with the prefix 'B' and 'R' corresponding to the brookite and rutile phases, respectively. An important feature of the diffraction pattern is that the intensity ratios of the different Bragg reflections from a particular crystallographic phase are quite different from that of reported powder diffraction patterns. This clearly indicates that the titania crystallites in the lipid matrix are oriented with specific crystallographic planes parallel to the substrate. It is observed that oriented growth of the brookite phase along the (112) and (212) directions has taken place. The commonly observed products of hydrolysis of titanium compounds<sup>26–32</sup> in solution are anatase and rutile.

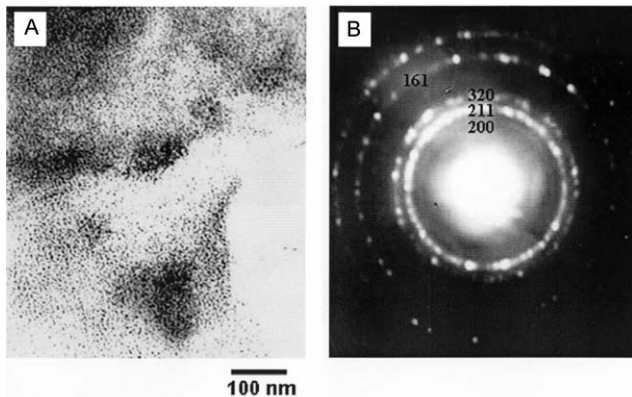


**Fig. 3** (A) Representative TEM micrograph of titania nanoparticles synthesized within a 250 Å ODA thin film (see text for details). (B) SAED pattern recorded for titania nanoparticles synthesized within the 250 Å ODA thin film.

reflections with a characteristic odd–even intensity oscillation that is symptomatic of lamellar c-axis ordering of the titanium ions in the ODA matrix.<sup>14</sup> From the separation between the (00l) Bragg reflections, the bilayer thickness in the ODA– $\text{TiF}_6$  composite was calculated to be *ca.* 50.9 nm. This repeat distance is in good agreement with the dimensions of the ODA molecule and the  $\text{TiF}_6^{2-}$  complex. The XRD pattern recorded from the ODA– $\text{TiF}_6$  composite film after hydrolysis is shown in the main part of Fig. 4. It can be seen from this figure that there are a number of Bragg reflections (which were absent prior to the hydrolysis step) indicating that the titania nanoparticles are quite crystalline. Analysis of the diffraction pattern indicated that the Bragg reflections correspond mostly to the brookite phase and to a small extent to the rutile phase. The various Bragg reflections have been indexed in Fig. 4 with the prefix 'B' and 'R' corresponding to the brookite and rutile phases, respectively. An important feature of the diffraction pattern is that the intensity ratios of the different Bragg reflections from a particular crystallographic phase are quite different from that of reported powder diffraction patterns. This clearly indicates that the titania crystallites in the lipid matrix are oriented with specific crystallographic planes parallel to the substrate. It is observed that oriented growth of the brookite phase along the (112) and (212) directions has taken place. The commonly observed products of hydrolysis of titanium compounds<sup>26–32</sup> in solution are anatase and rutile.

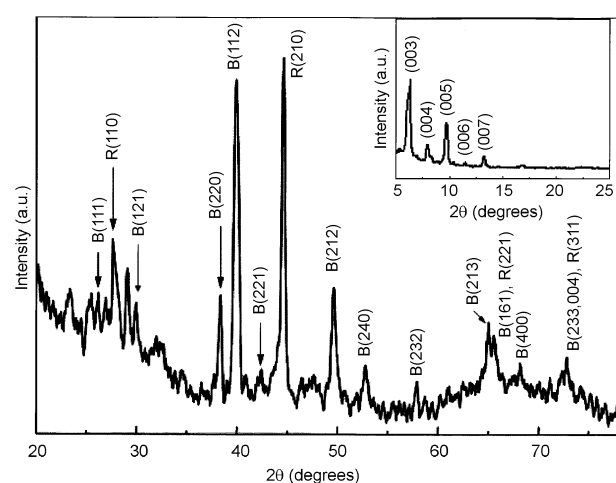


**Fig. 4** XRD pattern of an ODA composite thin film after hydrolysis of entrapped  $\text{TiF}_6^{2-}$  anions with 1% ammonia solution. The inset represents the XRD pattern just after entrainment of  $\text{TiF}_6^{2-}$  anions into the 250 Å thick ODA film indicating lamellar ordering within the film with a periodicity of *ca.* 50.9 nm.

In some cases, brookite is observed as a by-product when the hydrolysis of titanium complexes is carried out in an acidic medium at low temperatures<sup>30,31,33,34</sup> or when the precipitate formed from  $TiCl_4$  and ammonia is aged for a 15 month period.<sup>35</sup> Classically, brookite is obtained as large crystals by hydrothermal methods at high temperatures and pressures ( $200 \leq T \leq 400$  °C,  $10 \leq P \leq 400$  bar) in aqueous<sup>36</sup> or in organic media.<sup>37</sup> It has been reported that presence of some alkaline and alkaline earth metal ions induce formation of the brookite phase. Though sodium has been observed to produce in some cases pure brookite phase, potassium has been observed to result in a mixture of brookite and anatase forms.<sup>37</sup> In this study, we obtain a mixed phase of brookite and rutile unlike in the above report where the second phase obtained was anatase. The most interesting feature of the titania nanoparticle synthesis procedure described in this paper is that even under basic and very mild temperature conditions (50 °C), the ODA film is able to favor the formation of brookite rather than the more stable forms, anatase and rutile. Oriented growth of the brookite nanocrystals as discussed above indicates that there is some degree of epitaxy between specific crystallographic faces of this polymorph and the ODA bilayer template, thus stabilizing the brookite phase. Other possibilities for stabilizing the brookite phase include the presence of potassium ions within the interlamellar regions of the ODA bilayer structure and a locally acidic environment that arises due to the presence of  $F^-$  ions released during the conversion of  $TiF_6^{2-}$  ion to its oxide form in the film.

In conclusion, we have shown that electrostatic entrapment of  $TiF_6^{2-}$  ions within fatty amine thin films provides an efficient route for the synthesis of titania nanoparticles with a fair degree of size control. The titania nanoparticles grow predominantly in the brookite polymorph and are apparently stabilized by the fatty amine matrix. Combining this approach with more efficient chemical procedures or other techniques to form patterned structures of fatty amine thin films should provide a great variety of intricate nanoparticulate structures. Currently, extension of this methodology to the synthesis of nanoparticles of zirconia and ternary/doped oxides is being attempted.

## Acknowledgements

S. S. S. thanks the Council of Scientific and Industrial Research (CSIR), Govt. of India, for financial assistance. D. R. thanks the Department of Science and Technology (DST), Government of India for a project assistantship. This work was partially funded by grants to M. S. from the DST and the Indo-French Centre for the Promotion of Advanced Scientific Research (IFCPAR, New Delhi) and is gratefully acknowledged.

## References

- 1 B. O'Regan and M. Grätzel, *Nature*, 1991, **353**, 737–739.
- 2 A. Fujishima and K. Honda, *Nature*, 1972, **238**, 37–38.
- 3 A. Chemseddine and H. P. Boehm, *J. Mol. Catal.*, 1990, **60**, 295.
- 4 A. Mills and S. L. Hunte, *J. Photochem. Photobiol. A*, 1997, **108**, 1–35.
- 5 M. R. Hoffmann, S. T. Martin, W. Choi and D. W. Bahnemann, *Chem. Rev.*, 1995, **95**, 69–96.
- 6 Y. Takahashi, A. Ogiso, R. Tomoda, K. Sugiyama, H. Minoura and M. Tsuiki, *J. Chem. Soc., Faraday Trans. 1*, 1982, **78**, 2563.
- 7 M. Ferroni, V. Guidi, G. Martinelli, P. Nelli and G. Sberveglieri, *Sens. Actuators B: Chemical*, 1997, **44**, 499–502.
- 8 G. Wille, J. N. Rao and D. Fitzmaurice, *J. Mater. Chem.*, 1999, **9**, 2297–2299.
- 9 C. Bechinger, S. Ferrere, A. Zaban, J. Sprague and B. A. Gregg, *Nature*, 1996, **383**, 608.
- 10 S. Y. Huang, L. Kavan, I. Exnar and M. Grätzel, *J. Electrochem. Soc.*, 1995, **142**, L142–143.
- 11 A. N. Shipway, E. Katz and I. Willner, *ChemPhysChem*, 2000, **1**, 18–52.
- 12 X. Zhao, S. Xu and J. H. Fendler, *J. Phys. Chem.*, 1990, **94**, 2573.
- 13 D. V. Paranjape, M. Sastry and P. Ganguly, *Appl. Phys. Lett.*, 1993, **63**, 18.
- 14 P. Ganguly, M. Sastry, S. Pal and M. N. Shashikala, *Langmuir*, 1995, **11**, 1078.
- 15 S. Mandal, S. R. Sainkar and M. Sastry, *Nanotechnology*, 2001, **12**, 358.
- 16 S. Mandal and M. Sastry, *Mater. Res. Bull.*, 2002, **37**, 1613.
- 17 S. Mandal, C. Damle, S. R. Sainkar and M. Sastry, *J. Nanosci. Nanotechnol.*, 2001, **1**, 281.
- 18 M. Sastry, M. Rao and K. N. Ganesh, *Acc. Chem. Res.*, 2002, **35**, 847, and references therein.
- 19 P. Lobl, M. Huppertz and D. Mergel, *Thin Solid Films*, 1994, **251**, 72.
- 20 H. K. Ha, M. Yosimoto, H. Koinuma, B. Moon and H. Ishiara, *Appl. Phys. Lett.*, 1996, **68**, 2965.
- 21 Y. Takahashi, S. Wakayama, A. Ogiso and K. Sugiyama, *Kinzoku Hyomen Gijutsu*, 1984, **35**, 584.
- 22 L. D. Arsov, W. Kormann and W. Plieth, *J. Raman Spectrosc.*, 1991, **22**, 573.
- 23 L. D. Arsov, W. Kormann and W. Plieth, *J. Electrochem. Soc.*, 1991, **138**, 2964.
- 24 G. Z. Sauerbrey, *Z. Phys. (Munich)*, 1959, **155**, 206.
- 25 P. M. Kumar, S. Badrinarayanan and M. Sastry, *Thin Solid Films*, 2000, **358**, 122.
- 26 E. Santacesaria, M. Tonello, G. Storti, R. C. Pace and S. J. Carra, *J. Colloid Interface Sci.*, 1986, **111**, 44.
- 27 E. Matijevic, M. Budnick and L. Meites, *J. Colloid Interface Sci.*, 1977, **61**, 302.
- 28 L. I. Bekker, I. P. Dobrovolskii and A. A. Ivakin, *Russ. J. Inorg. Chem.*, 1976, **21**, 223.
- 29 A. Chemseddine and T. Moritz, *Eur. J. Inorg. Chem.*, 1999, **2**, 235.
- 30 B. L. Bischoff and M. A. Anderson, *Chem. Mater.*, 1995, **7**, 1772.
- 31 P. Arnal, J. P. R. Corriu, D. Leclercq, P. H. Mutin and A. Vioux, *J. Mater. Chem.*, 1996, **6**, 1925.
- 32 P. Arnal, J. P. R. Corriu, D. Leclercq, P. H. Mutin and A. Vioux, *Chem. Mater.*, 1997, **9**, 694.
- 33 S. Music, M. Gotic, M. Ivanda, S. Popovic, A. Turkovic, R. Trojko, A. Sekulic and K. Furie, *Mater. Sci. Eng., B*, 1997, **47**, 33.
- 34 X. Bokhimi, A. Morales, O. Novaro, T. Lopez, E. Sanchez and R. Gomez, *J. Mater. Res.*, 1995, **10**, 2788.
- 35 J. P. Jalava, L. Heikkila, O. Hovi, R. Laiho, E. Hiltunen, A. Hakanen and H. Harma, *Ind. Eng. Chem. Res.*, 1998, **37**, 1317.
- 36 I. Keesmann, *Z. Anorg. Allg. Chem.*, 1966, **346**, 31.
- 37 H. Kominami, M. Kohno and Y. Kera, *J. Mater. Chem.*, 2000, **10**, 1151.